DERIVING SPATIAL STABILITY VARIATIONS FROM PENETRATION RESISTANCE MEASUREMENTS

Sascha Bellaire* and Jürg Schweizer
WSL Institute for Snow and Avalanche Research SLF, Davos

ABSTRACT: Spatial variations of weak layer and slab properties affect snow slope stability. To quantify spatial variability at the slope scale, penetration resistance was measured with a high resolution snow-micro penetrometer (SMP) in a partly randomized grid pattern. The design consisted of 46 measurement locations and was optimized for geostatistical analysis. In addition, a full snow profile and 20 compression tests were performed within the grid. Stability test results were compared to stability information derived from the SMP signal using a recently developed algorithm. A dataset consisting of five grids done fortnightly on a southwest facing slope was analysed. A layer of facets was the predominant weak layer and was identified by the algorithm in most cases. The stability patterns derived from the compression tests were mostly reproduced by the stability formulation of the algorithm. Changes of slab properties seemed to be a major cause for changes in slope stability over time. The spatial stability variation was derived from a indicator semivariogram. Based on the resulting range and nugget ratio a scheme for estimating slope stability was proposed.

KEYWORDS: snow mechanical properties, snow stability, avalanche formation, spatial variability, geo-statistics

1. INTRODUCTION

Spatial variations of weak layer and slab properties are considered a key factor for snow slope stability. Spatial variability is presumably caused by meteorological conditions such as wind and radiation, as well as metamorphic processes (Schweizer et al., 2008). Kronholm and Schweizer (2003) suggested slope stability to be related to the degree of stability variation, the length scale of variation and the mean point stability. Previous studies analysed layer properties at the slope scale (Kronholm and Schweizer, 2003, Birkeland et al., 2004). Layers were often spatially continuous and showed less variability than the stability of small column tests.

The snow micro-penetrometer (SMP) developed by Schneebeli and Johnson (1998) measures high resolution penetration resistance and allows to derive micro-structural snow parameters. Pielmeier et al. (2006) related snow layer properties derived from the SMP to point stability by analysing a series of individual manual snow profiles in conjuncture with an SMP measurement. Kronholm and Schweizer (2003) were unable to relate spatial SMP measurements to the manual stability observations partly due to (a) the sampling design that did not allow a geostatistical analysis for the manual stability observations and (b) the lack of an SMP derived stability parameter. Recently, Bellaire et al. (2008) have developed an algorithm for analysing the SMP signal with the aim to detect potential weak layers and estimate the probability of triggering.

We will analyse a series of spatial measurements at the slope scale of penetration resistance (SMP) and point stability (compression test) performed about fortnightly on a south-west facing slope near Davos, Switzerland. The aim is to derive stability patterns and relate them to slope stability.

Corresponding author address: Sascha Bellaire, WSL Institute for Snow and Avalanche Research SLF, Flüelastrasse 11,
CH-7260 Davos Dorf, Switzerland;
tel: +41 81 4170292; fax: +41 81 4170110;
email: bellaire@slf.ch

2. METHODS

2.1 Snow micro-penetrometer (SMP)

Schneebeli and Johnson (1998) developed a snow micro-penetrometer (SMP) for high resolution (in space and time) snow cover investigations. The SMP is a cone-shaped probe which is driven into the snow cover by a motor at a constant speed of 20 mm s^{-1}. Penetration resistance is measured every 4 μm by a piezo-electric force sensor.

Johnson and Schneebeli (1999) developed a microstructural model to derive microme-

chanical properties of snow from the SMP signal. A microstructural element will rupture within a typical length of dimension L_n, and will induce a peak force in the SMP signal F_{max}. The rupture force f_r is the force needed to rupture the crystal structure, i.e. a bond. The number of ruptures per unit length is defined as the number of peaks n_{peaks}. Figure 1 illustrates these three parameters for two different snow types.

The peak force and the number of ruptures are typically larger for small rounded grains (non-persistent grain type) than for depth hoar (persistent grain type), a typical weak layer (Schneebeli et al., 1999).

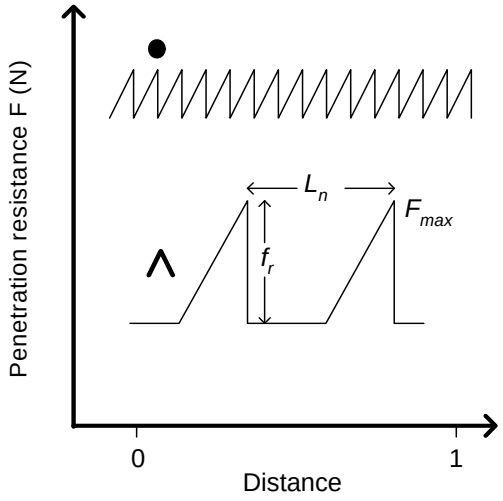

Figure 1: Schematic SMP signals for small rounded grains (top) and depth hoar (bottom), and the definition of the microstructural parameters, rupture force f_r, element length L_n and peak force F_{max}. The number of peaks n_{peaks} corresponds the number of ruptures per unit length.

2.2 Partly randomized sampling design

To quantify spatial variability, measurements of snow cover properties need to be performed spatial distributed on potential avalanche slopes. For spatial analysis geostatistics has been used to identify spatial structure and correlation length of snow properties responsible for avalanche formation (e.g. Kronholm.) An optimized sampling design enables to identify the spatial structure with a minimum of measurements. If the correlation length is unknown, then the sampling design should contain some randomness (Kronholm and Birkeland, 2007). However, in practice, randomly distributed measurement points are difficult to locate on grids where the extent (maximal distance between measurement points) is small (≤ 20 m), i.e. locating points, for example, by GPS is impossible.

The sampling design used in this study was developed for a grid of 18 m × 18 m (Figure 2). This area was divided into nine sub-grids of 6 m × 6 m. Each sub-grid contains 5 SMP measurements in a L-shaped order (Cline et al., 2001). The spacing between each SMP measurement differs (0.25 m, 0.5 m, 1 m). This sampling design has well distributed lag distances h (distances between measurement locations), with a mean lag distance of 9 m and a extent of 19 m. Additionally, each sub-grid contained two compression test locations left and right from the SMP measurement (20 in total). Furthermore, a manually observed snow profile, including an additional SMP profile next to it, and a rutschblock test and two compression tests were performed within a grid.

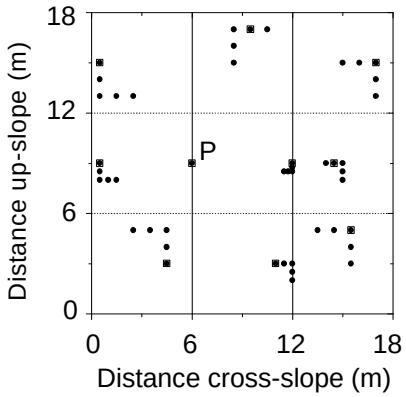

Figure 2: Sampling design optimized for geostatistics. Dots indicate locations of SMP measurements, squares location of compression tests additionally to the SMP measurement. P indicates the position of the manual profile and the rutschblock and two additionally compression tests.

2.3 SMP signal analysis

We used an algorithm recently developed by Bellaire et al. (2008, submitted) to extract stability information from the SMP signal. The algorithm identifies the potential weak layer and estimates the probability of triggering by a stepwise sequential analysis of the SMP signal. In a first step, a structural parameter Ψ was defined:

$$\Psi = \frac{\bar{f}_r \, n_{peaks}}{A} \qquad (1)$$

with the mean rupture force $\bar{f}_r$, averaged over one millimetre of the signal, n_{peaks} the number of ruptures and A the surface area of the sensor tip (A = 39 mm^2). Schweizer and Jamieson (2003) found that large discontinuities in structure indicate weak layers or interfaces. Consequently, a second structural parameter Δ was defined:

$$\Delta = \frac{A \; grad \; \Psi}{F_{\max}} \, w(z) \qquad (2)$$

where *w(z)* is a depth dependent weighting function. Potentially weak layers or transitions are identified by locating the four extreme values of Δ. To identify the layer boundaries the gradient of the coefficient of variation (COV) of the force signal was calculated (Spiegel and Stephens, 1999). A layer boundary was defined as the position where the gradient of the COV is larger than 0.1 (defined empirically). These positions above and below the four extreme values of Δ are defined as upper and lower boundary, respectively.

Finally, a stability parameter S was defined:

$$S = \frac{F_{\max}}{\bar{F}_{WL}} \Psi \qquad (4)$$

with F_{max} the maximum penetration resistance within the slab, and $\bar{F}_{wl}$ the mean penetration resistance from the upper to lower boundary of the weak layer. Values of $S \leq 190.4 \times 10^3$ N^2 m^{-2} indicated rather unstable conditions and were assigned the stability class “poor”, and “fair-to-good”, alternatively.

Bellaire et al. (2008, submitted) compared the failure layer depth identified with the above described algorithm to the observed failure layer depth for 68 profiles. In 88% of the cases the weak layer corresponded to one of the four potential weak layers identified by Δ. These SMP profiles were classified into the two stability classes with an accuracy of 75% - provided one of the four potential weak layers was selected manually as the critical one.

2.4 Measurements and manual observations

As described above each grid consisted of 46 SMP measurements and 10 pairs of compression tests. We used the minimum score of the two compression tests (done side by side) for further analysis. The compression test scores where classified into two stability classes of “poor” and “fair-to-good” following Schweizer and Jamieson (2003). Compression test scores ≤ 13 were classified as poor, and >13 as fair-to-good.

The 46 SMP measurements were analysed using the above described algorithm for weak layer detection and stability estimation. For each sub-grid a mean stability was defined by taking the median stability from all SMP measurements of the sub grid. This mean stability was than compared to the stability test result of the corresponding compression test.

2.4 Data analysis

To quantify the differences between the stability derived from the compression test and the stability estimated by the algorithm, spatial as well as non-spatial statistics were used. For the spatial analysis we calculate the sum of absolute differences (SAD) defined as:

$$SAD = \frac{1}{N} \sum \left(\left| S_{CT} - S_{SMP} \right| \right) \qquad (5)$$

with S_{CT} and S_{SMP} the stability at corresponding grid locations derived by the compression test and the SMP, respectively. SAD = 0 indicates a perfect match between all grid locations.

The non-spatial statistics were done by cross-tabulating the stability estimates and calculating a Yates’ corrected Pearson χ^2 statistic (Spiegel and Stephens, 1999). A level of significance p=0.05 was chosen to decide whether the differences were statistically significant.

To determine the spatial structure of a grid an experimental indicator semi-variogram (Goovaerts, 1997) was calculated by:

$$\gamma(h) = \frac{1}{2m(h)} \sum_{i=1}^{m(h)} \{ Z_{ind}(x_i) - Z_{ind}(x_i + h) \}^2 \qquad (6)$$

with *m(h)* the number of point pairs separated by the lag distance h, and $x_i=(X_i,Y_i)$ the location of the measurements. Z_{ind} is the indicator variable, which is 0 for rather unstable (“poor”) and 1 for rather stable (“fair-to-good”) conditions. By fitting a spherical model to the experimental semivariogram we determined the sill σ^2, range R, and the nugget τ as well as the nugget ratio $\alpha=\tau/\sigma^2$ (Webster and Oliver, 2007). When no range could be identified by the model the range R was assumed to be ≥ 19 m, i.e. the maximal extent.

3. DATA

We analysed 5 grids on a south-west facing slope above timberline (2450 m a.s.l) in the region of Davos, Switzerland. The predominant weak layer on the slope was a layer of depth hoar. The grids were done within 4 hours about fortnightly from January to March 2008.

The slope stability was estimated at end of the field day based on any sign of instability such as “whumpfs” or recent avalanche activity on nearby slopes. We recorded and reported this stability estimate (expressed as the danger level) on a regular basis. During the observation period, from grid 1 to 5, snowpack stability generally improved.

4. RESULTS

The comparison between the observed stability (compression test results) and the stability estimated by the algorithm from the SMP signal is shown in Figure 3. Table 1 summarises the results of the spatial and non-spatial analysis.

The non-spatial analysis shows no significant differences between the stability derived from the SMP and the observed stability (CT) for all grids. The largest deviation is observed for grid 3. The spatial statistics (SAD) indicated that usually in 6 or more (out of 10) locations the stability estimate agreed with the stability observed with the compression test. Figure 3 suggests that many of the stability patterns can be found in both the stability estimated from the SMP and the stability observed with the CT.

Table1: Comparison between stability derived from compression tests and the stability derived from the SMP. The sum of absolute differences (SAD) (spatial statistics) and the *p*-value (non-spatial statistics) are given together with the rutschblock (RB) score, the slope median compression test (CT) score and the estimated slope stability for each grid.

Grid No.	RB	CT	Slope stability	*p*-value	SAD
1	2	10.5	poor-to-fair	1	0
2	2	11	poor	1	0.1
3	4	12.5	poor-to-fair	0.14	0.4
4	3	14	fair-to-good	0.63	0.4
5	6	16.5	fair	0.65	0.2

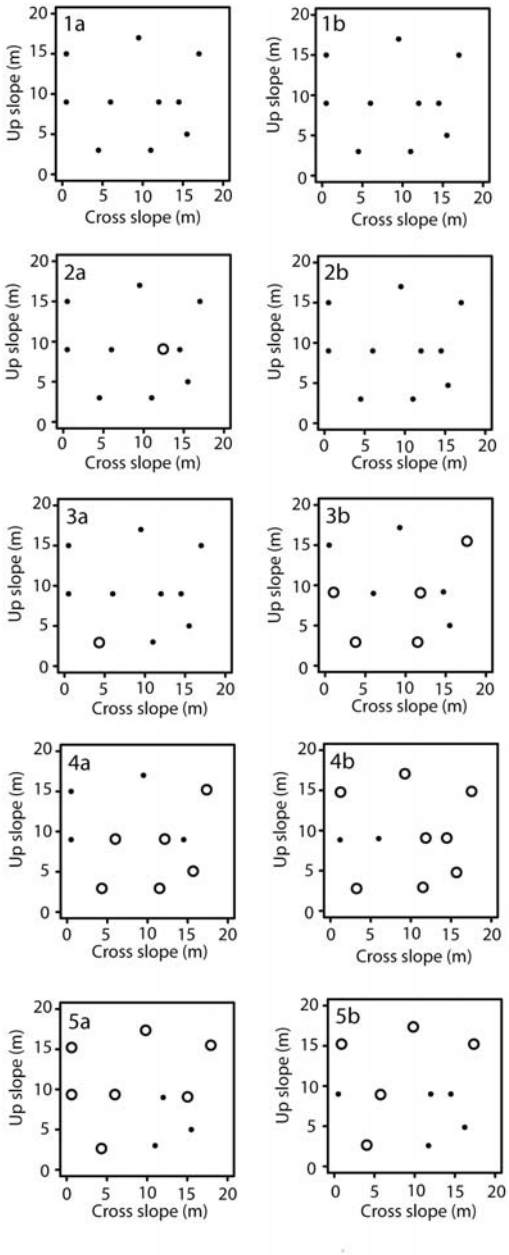

Figure 3: Comparison between (a) observed stability (CT) and (b) estimated stability by the SMP algorithm for grids 1 to 5. Dots indicate poor, open circles fair-to-good snowpack conditions.

The weak layer penetration resistance and the maximum penetration resistance of the slab derived from the SMP are shown in Figure 4. The penetration resistance of the weak layer decreased from grid 1 to 2 and subsequently increased up to grid 5. The maximum penetration resistance in the slab was considerably higher for grids 3 to 5 than for grids 1 to 2.

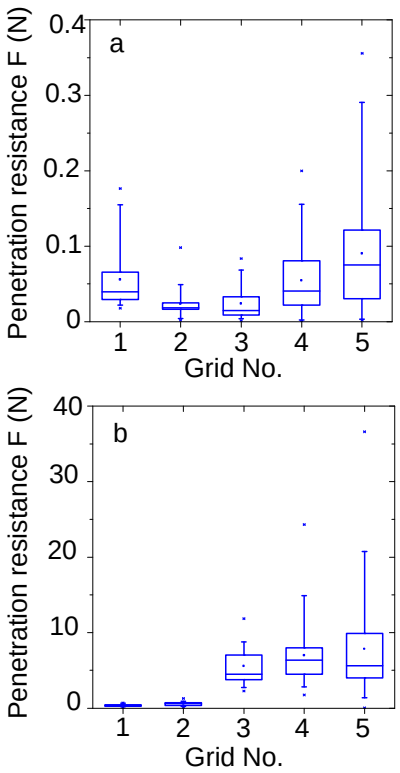

Figure 4: (a) Distribution of weak layer penetration resistance derived from the SMP for grids 1 to 5 and (b) distribution of maximum penetration resistance of the slab for grids 1 to 5. Boxes span the interquartile range from 1st to 3rd quartile with the horizontal line showing the median. Whiskers show the range of observed values that fall within 1.5 times the interquartile range above and below the interquartile range. Outlier are marked with asterisk.

Table 2 shows the correlation length (range) R, sill σ^2, nugget τ and the nugget ratio α derived from a spherical indicator semivariogram model for grid 1 to 5, as well as the ratio of the range to a critical range assumed to be about 10 m (Schweizer, 1999). The geostatistical results for the SMP measurements suggest a decreasing range R and a increasing sill σ^2 with time, i.e. from grid 1 to 5.

Based on the semivariogram values range R, sill σ^2 and nugget τ, summarized in Table 2, a stability scheme is suggested (Figure 5). Slopes can be classified into various stability classes depending on the mean point stability, the range of autocorrelation in relation to a critical failure length and the nugget ratio. The scheme is based on the proposal by Kronholm and Schweizer (2003) but now uses measured geostatistical parameters.

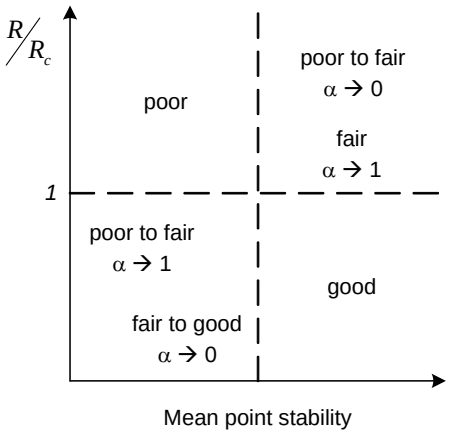

Figure 5: Schematic for slope stability classification based on the ratio of correlation length (range R) to a critical failure length R_c, mean point stability, and the nugget ratio α as a measure of point stability variation.

5. DISCUSSION

Stability patterns at the slope scale derived by compression tests were partly reproduced by a recently developed stability algorithm to analyse SMP signals. However, both the stability derived from compression tests as well as the estimated stability from the SMP signals are prone to errors.

The compression test scores can be affected by not uniform columns and inconsistent taping. Furthermore, the comparison was done by classifying the compression test scores into two stability classes based on a threshold value CT ≤ 13, i.e. the uncertainty of the compression test result affects the stability classification, in particular if close to the threshold value. This might partly explain the mismatch in grid 3 (median compression test score was 12.5, RB score was 4). The SMP stability estimate is prone to measurement errors and limitations of the algorithm, which will also affect the stability pattern.

The maximal measured penetration resistance of the slab seems to be an indicator for slope stability. Large values were associated with rather stable conditions. Manual observations showed thick melt-freeze crusts within the slab when grids 3 to 5 were performed. The weak layer penetration resistance from the grids classified as poor to the grids classified as fair-to-good. However, limitations of the algorithm in particular on how layer boundaries are defined may effect the mean weak layer penetration resistance.

Table 2: Results of the geostatistical analysis for all 5 grids for CT stability and SMP stability. Range R derived from a fitted indicator semivariogram model and the ratio of R to a critical length R_c (10 m), as well as the sill σ^2, the nugget τ and the nugget ratio α are given.

Grid No.	CT					SMP					Slope stability estimate
	R (m)	σ^2	τ	α	R/R_c	R (m)	σ^2	τ	α	R/R_c	
1	≥19	0.1	0.1	1.00	≥1.9	≥19	0.1	0.1	1.00	≥1.9	poor-to-fair
2	15.6	0.11	0.11	1.00	1.6	≥19	0.1	0.1	1.00	≥1.9	poor
3	12.5	0.11	0.11	1.00	1.3	15.6	0.29	0.29	1.00	1.6	poor-to-fair
4	16.2	0.26	0.22	0.85	1.6	10.5	0.29	0.1	0.34	1.1	fair-to-good
5	16.2	0.24	0.19	0.79	1.6	11.0	0.41	0.1	0.24	1.1	fair

We analysed five consecutive arrays. During the time the measurements were done slope stabilisation was observed. In general, it is not possible to decide whether a slope is unstable, unless it is triggered. Occasionally, we observed "whumpfs" while approaching or working on the slope which is not steep enough to slide. Slope stability is therefore an estimate based on any sign of instability we were able to observe in the region on the day of our field work. As a result, observed slope stability should be interpreted as a trend only towards either rather unstable or stable conditions, respectively. More observations on different slopes and aspects would be needed to validate the proposed slope stability classification scheme.

6. CONCLUSIONS

We analysed spatial measurements of penetration resistance (SMP) and stability (CT) that were performed using a partly randomized grid design on a south-west facing slope near Davos, Switzerland. A recently developed algorithm to derive stability from the SMP signal was used and results suggest rather good agreement with observed stability (CT). From grid 1 to 5 the slope in general stabilized in accordance with increasing compression test scores and increasing number of SMP signals that were classified as rather stable (fair-to-good). General stability patterns observed with the compression test were mostly reproduced by the SMP stability. The causes of these spatial patterns are still unknown. Geostatistical analyses suggested a relation between the range, sill and the nugget-ratio, and slope stability. The proposed classification scheme has to be considered as preliminary and more data will be needed to link spatial patterns expressed with geostatistical parameters to slope instability and avalanche formation in general.

Our results suggest that the SMP – still supplemented with some manual observations – has promising potential for snow cover investigations where high resolution data are required.

ACKNOWLEDGEMENTS

For help with the field work we would like to thank Alec van Herwijnen and Christoph Mitterer, as well as Sina Schneider, Michael Schirmer, and Charles Fierz. We gratefully acknowledge financial support by the European Commission (FP6-STReP-NEST, Project no. 043386: TRIGS).

REFERENCES

Bellaire, S., C. Pielmeier, M. Schneebeli, and J. Schweizer, 2008: Stability algorithm for snow micro-penetrometer measurements. *J. Glaciol.*, submitted.

Birkeland, K., K. Kronholm, M. Schneebeli, and C. Pielmeier, 2004: Changes in shear strength and micropenetration hardness of a buried surface-hoar layer. *Ann. Glaciol.*, **38**, 223-228.

Cline, D., R. Armstrong, R. Davis, K. Elder, and G. Liston, 2001. NASA Cold Land Processes Field Experiment Plan. [Available online at http://www.nohrsc.nws.gov/~cline/clpx.html]

Goovaerts, P., 1997. *Geostatistics for natural resources evaluation*. Applied geostatistics series. Oxford University Press, New York. 483 pp.

Johnson, J.B. and M. Schneebeli, 1999: Characterizing the microstructural and micromechanical properties of snow. *Cold Reg. Sci. Technol.*, **30**(1-3), 91-100.

Kronholm, K., 2004: Spatial variability of snow mechanical properties with regard to avalanche formation, Ph.D. Thesis, University of Zurich, Zurich Switzerland, 192pp.

Kronholm, K. and K. W. Birkeland, 2007: Reliability of sampling designs for spatial snow surveys. *Comput. Geosci.*, **33**(9), 1097-1100.

Kronholm, K. and J. Schweizer, 2003: Snow stability variation on small slopes. *Cold Reg. Sci. Technol.*, **37**(3), 453-465.

Pielmeier, C., J. Schweizer, and H.P. Marshall, 2006: Improvements in the application of the SnowMicroPen to derive stability information for avalanche forecasting. *Proceedings ISSW 2006. International Snow Science Workshop, Telluride CO, U.S.A., 1-6 October 2006*, 187-192.

Schneebeli, M. and J.B. Johnson, 1998: A constant-speed penetrometer for high-resolution snow stratigraphy. *Ann. Glaciol.*, **26**, 107-111.

Schneebeli, M., C. Pielmeier, and J.B. Johnson, 1999: Measuring snow micro structure and hardness using a high resolution penetrometer. *Cold Reg. Sci. Technol.*, **30**(1-3), 101-114.

Schweizer, J., 1999. Review of dry snow slab avalanche release. *Cold Reg. Sci. Technol*., **30**(1-3), 43-57.

Schweizer, J. and J.B. Jamieson, 2003: Snowpack properties for snow profile analysis. *Cold Reg. Sci. Technol.*, **37**(3), 233-241.

Schweizer, J., K. Kronholm, J.B. Jamieson, and K.W. Birkeland, 2008. Review of spatial variability of snowpack properties and its importance for avalanche formation. *Cold Reg. Sci. Technol.*, **51**(2-3), 253-272.

Spiegel, M.R. and L.J. Stephens, 1999: *Schaum's outline of theory and problems of statistics*. 3rd ed. *Schaum's outline series*, McGraw-Hill, New York, 538 pp.

Webster, R. and M.A. Oliver, 2007. *Geostatistics for environmental scientists.* Statistics in Practice Wiley, Chichester. 315 pp.